Transport properties of a hybrid Majorana wire-quantum dot system with ferromagnetic contacts

I. Weymann* and K. P. Wójcik
Faculty of Physics, Adam Mickiewicz University, ul. Umultowska 85, 61-614 Poznań, Poland
(Received 29 January 2017; published 18 April 2017)

The transport properties of a quantum dot coupled to ferromagnetic contacts and attached to a topological superconductor wire hosting Majorana zero-energy modes at its ends are studied theoretically in the Kondo regime. By using the numerical renormalization group method, the temperature and dot level dependence of the spectral function, the conductance, and its spin polarization are studied for different coupling strengths to a topological superconductor. It is shown that the transport characteristics are generally determined by the interplay of three competing energy scales, resulting from Kondo correlations, a ferromagnetic-lead-induced exchange field, and topological-wire-induced splitting. These two splittings are found to have opposite signs. Moreover, they can compensate for each other in an appropriate parameter regime.

DOI: 10.1103/PhysRevB.95.155427

I. INTRODUCTION

Topologically protected states of matter are now at the forefront of condensed matter physics [1,2]. This is because such states are protected against many noise sources by symmetry, and they are thus naturally suited for operations in which decoherence is one of the main issues. One such prominent example is topological quantum computation [3,4], for which Majorana zero-energy modes [5], exhibiting non-Abelian statistics, are expected to play an important role. In fact, the signatures of Majorana fermions in solid-state devices have recently been observed experimentally [6–9].

In particular, much attention has been paid to hybrid Majorana quantum-dot systems, which typically consist of a quantum dot coupled to external leads and additionally attached to topological superconductor (TS) wire, which hosts Majorana zero-energy modes at its ends (Majorana wire). This is because such hybrid quantum-dot devices reveal some unique features related to the presence of Majorana quasiparticles [10–24]. For example, it was predicted [15] that the well-established Kondo effect in quantum dots [26–29] becomes modified by the presence of coupling to Majorana zero-energy modes in such a way that the low-temperature conductance reaches a fractional value of $3e^2/2h$ instead of $2e^2/h$. Moreover, out of the Kondo regime the conductance was shown to reach a value of $e^2/2h$ due to the coupling to Majorana wire [16]. Interestingly, very recently a hybrid Majorana wire-quantum dot device was realized experimentally, and the emergence of Majorana bound states was confirmed. It was achieved by performing bias spectroscopy, in which a quantum dot served as a spectrometer of Majorana zero-energy modes [25]. This exciting experiment undoubtedly paves the way toward more elaborate experimental realizations involving quantum dots and topological wires with Majorana quasiparticles. From this perspective, providing further theoretical modeling and understanding of Majorana quantum-dot systems is desirable.

In this paper, therefore, we undertake further studies on quantum dots side-coupled to Majorana wires in the Kondo regime, focusing on the case of ferromagnetic (FM) contacts; see Fig. 1 for a schematic of the considered system. We note that the transport properties of strongly correlated quantum dots coupled to magnetic leads have been a subject of intensive theoretical and experimental research for more than a decade [30–39]. In particular, it was demonstrated that the Kondo effect can be suppressed by the presence of an exchange field generated by spin-dependent couplings, which results in spin-splitting of the dot level [30,37]. Here, we show that in the presence of additional coupling to Majorana wire, the transport behavior becomes greatly modified. First of all, this coupling results in a splitting of the dot level, which has an opposite sign to the splitting caused by the exchange field coming from ferromagnetic leads. Consequently, we demonstrate that, depending on the device parameters, one can reinstate the Kondo effect, which was initially suppressed. Moreover, it is shown that the interplay between the exchange field, coupling to Majorana wire, and Kondo correlations results in highly nontrivial spectral features that are revealed in the dot's local density of states, linear conductance, and current spin polarization. The calculations are performed with the aid of the numerical renormalization group (NRG) method [40], which is well-suited to address the strongly correlated regime of various complex quantum impurity systems. Using the NRG, we determine the transport characteristics as a function of dot-level position for different temperatures, couplings to Majorana wire and considering the cases of both infinite- and finite-length nanowire. The case of ferromagnetic contacts is contrasted

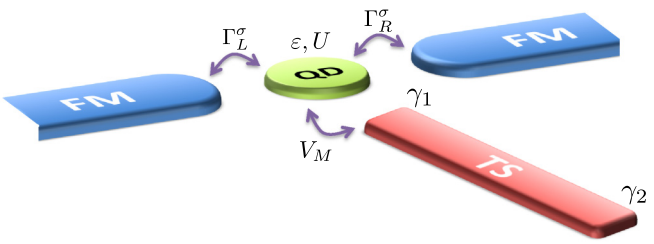

FIG. 1. The schematic of the considered system. It consists of a quantum dot (QD), with energy level ε and Coulomb correlations U, coupled to two ferromagnetic (FM) leads with coupling strengths Γ_L^σ and Γ_R^σ for the left and right junction, and side-coupled (with matrix element V_M) to a topological superconductor (TS) wire hosting two Majorana zero-energy modes described by the operators γ_1 and γ_2.

*weymann@amu.edu.pl

with the case of nonmagnetic leads, which helps in elucidating the role of spin-dependent tunneling on transport behavior.

II. THEORETICAL DESCRIPTION AND PERTURBATIVE ANALYSIS

A. Model

The considered system consists of a single-level quantum dot (QD) coupled to the left and right ferromagnetic (FM) leads, and side-coupled to a topological superconductor (TS) wire hosting Majorana zero-energy modes (Majorana wire) (see Fig. 1). The total Hamiltonian of the system has the following form:

$$H = H_{\rm leads} + H_{\rm DM} + H_{\rm tun}, \tag{1}$$

where $H_{\rm leads} = \sum_{r\mathbf{k}\sigma} \varepsilon_{r\mathbf{k}\sigma} c^\dagger_{r\mathbf{k}\sigma} c_{r\mathbf{k}\sigma}$ describes the noninteracting electrons in the left ($r = L$) and right ($r = R$) lead, with $c_{r\mathbf{k}\sigma}$ annihilating an electron of spin σ, momentum $\mathbf{k}$, and energy $\varepsilon_{r\mathbf{k}\sigma}$ in the lead r. The second term of H, $H_{\rm DM}$, represents the quantum dot coupled to a topological superconductor hosting Majorana zero-energy modes at its ends. Assuming the superconducting energy gap to be the largest energy scale, the QD-TS subsystem can be modeled by the following effective Hamiltonian [10,12,15]:

$$H_{\rm DM} = \varepsilon \sum_\sigma d^\dagger_\sigma d_\sigma + U d^\dagger_\uparrow d_\uparrow d^\dagger_\downarrow d_\downarrow + 2i\varepsilon_M \gamma_1 \gamma_2 + V_M (d^\dagger_\downarrow \gamma_1 + \gamma_1 d_\downarrow). \tag{2}$$

Here, d_σ is the annihilation operator of a spin-σ electron of energy ε in the dot, while U denotes the Coulomb interaction between two electrons of opposite spin occupying the dot. The operators γ_1 and γ_2 are related to the two Majorana fermions at the ends of the topological superconductor wire (see Fig. 1). These self-adjoint operators fulfill the anticommutation rule $\{\gamma_i, \gamma_j\} = \delta_{ij}$ and can be expressed in terms of an auxiliary fermionic operator f as $\gamma_1 = (f^\dagger + f)/\sqrt{2}$ and $\gamma_2 = i(f^\dagger - f)/\sqrt{2}$. The coupling between the topological superconductor and the quantum dot is described by the last term of $H_{\rm DM}$, where V_M is the respective tunnel matrix element. On the other hand, ε_M describes the overlap between the two Majorana fermions. In the limit of infinitely long topological superconductor wire, the two Majorana quasiparticles do not overlap, and $\varepsilon_M = 0$ [9]. Otherwise, $\varepsilon_M > 0$ can be assumed without a loss of generality. Finally, the last term of the total Hamiltonian (1) takes into account the coupling between the quantum dot and the leads,

$$H_{\rm tun} = \sum_{r\mathbf{k}\sigma} V_{r\sigma} (d^\dagger_\sigma c_{r\mathbf{k}\sigma} + c^\dagger_{r\mathbf{k}\sigma} d_\sigma), \tag{3}$$

where the tunnel matrix elements $V_{r\sigma}$ are assumed to be momentum-independent. Hybridization with the leads gives rise to a finite width of the dot level, $\Gamma = \sum_{r\sigma} \Gamma^\sigma_r$, where $\Gamma^\sigma_r = \pi \rho^\sigma_r V^2_{r\sigma}$, with ρ^σ_r denoting the spin-dependent density of states of lead r. The spin-dependent coupling strength can be written as $\Gamma^\sigma_r = (1 + \sigma p_r)\Gamma_r$, with $\Gamma_r = (\Gamma^\uparrow_r + \Gamma^\downarrow_r)/2$ and p_r denoting the spin polarization of lead r. We assume a left-right symmetric system, $\Gamma_L = \Gamma_R = \Gamma/2$ and $p_L = p_R = p$. We also assume a flat density of states of the leads and use its half-width as the energy unit. Moreover, it is important to notice that in general the magnetic moments of the leads and the spin in the quantum dot need not be collinear. However, in the present work we assume that they are aligned along the same quantization axis.

B. Isolated Majorana quantum-dot system

To begin with, let us discuss the properties of a quantum-dot–topological-wire subsystem decoupled from the normal leads. By noting that the Hamiltonian (2) commutes with the charge-parity operator P_Q and $n_\uparrow = d^\dagger_\uparrow d_\uparrow$, one can easily find its eigenspectrum [15,24]. In the singly occupied dot regime, $-U \ll \varepsilon \ll \Gamma$, the ground state for $\varepsilon > -U/2$ and $\varepsilon_M > 0$ is

$$|\Downarrow\rangle = -\alpha_+(x_\Downarrow) f^\dagger |0\rangle + \alpha_-(x_\Downarrow) d^\dagger_\downarrow |0\rangle, \tag{4}$$

where $|0\rangle$ denotes the vacuum state, $x_\Downarrow = \varepsilon/2 - \varepsilon_M$, and the coefficients $\alpha_\pm(x)$ are given by

$$\alpha_\pm(x) = \frac{1}{\sqrt{2}} \sqrt{1 \pm \frac{x}{\sqrt{x^2 + V_M^2/2}}}. \tag{5}$$

The corresponding eigenenergy equals $\varepsilon_\Downarrow = [\varepsilon - \sqrt{(\varepsilon - 2\varepsilon_M)^2 + 2V_M^2}]/2$. On the other hand, for $\varepsilon < -U/2$, the ground state becomes

$$|\Uparrow\rangle = -\alpha_+(x_\Uparrow) d^\dagger_\uparrow |0\rangle + \alpha_-(x_\Uparrow) d^\dagger_\uparrow d^\dagger_\downarrow f^\dagger |0\rangle, \tag{6}$$

where $x_\Uparrow = \varepsilon/2 + U/2 + \varepsilon_M$, and the eigenenergy is given by $\varepsilon_\Uparrow = [3\varepsilon + U - \sqrt{(\varepsilon + U + 2\varepsilon_M)^2 + 2V_M^2}]/2$. These two states are degenerate for $\varepsilon = -U/2$, otherwise the dot level becomes split due to the coupling to the Majorana zero-energy mode by $\delta\varepsilon_M \equiv \varepsilon_\Uparrow - \varepsilon_\Downarrow$, which is explicitly given by [15]

$$\delta\varepsilon_M = \varepsilon + \frac{U}{2} + \frac{1}{2}\sqrt{(\varepsilon - 2\varepsilon_M)^2 + 2V_M^2} - \frac{1}{2}\sqrt{(\varepsilon + U + 2\varepsilon_M)^2 + 2V_M^2}. \tag{7}$$

This splitting is plotted in Fig. 2(a) [Fig. 2(b)] against the quantum-dot energy level for different values of V_M and ε_M ($\varepsilon_M > 0$), respectively. Clearly, the dependence of $\delta\varepsilon_M$ on ε is monotonic, except for the case of $V_M = 0$, when obviously $\delta\varepsilon_M = 0$. In agreement with intuition, the splitting is enhanced by the growing coupling to the topological superconductor. Generally, $\delta\varepsilon_M$ can be quite well approximated as directly proportional to $\varepsilon - U/2$ close to the particle-hole symmetry point. For $\varepsilon_M = 0$ and in the leading order in V_M, it may be written as

$$\delta\varepsilon_M \approx \frac{4V_M^2}{U^2}\left(\varepsilon + \frac{U}{2}\right). \tag{8}$$

Moreover, it barely depends on ε_M for $\varepsilon_M \ll U$ [compare Figs. 2(a) and 2(b)].

In the limit of infinite-length Majorana wire ($\varepsilon_M \to 0$), the (spin-split) ground state described so far becomes degenerate. We note that the next relevant pair of states is

$$|\Uparrow^*\rangle = -\alpha_+(x_{\Uparrow *}) d^\dagger_\uparrow f^\dagger |0\rangle + \alpha_-(x_{\Uparrow *}) d^\dagger_\uparrow d^\dagger_\downarrow |0\rangle, \tag{9}$$

$$|\Downarrow^*\rangle = -\alpha_+(x_{\Downarrow *}) |0\rangle + \alpha_-(x_{\Downarrow *}) d^\dagger_\downarrow f^\dagger |0\rangle, \tag{10}$$

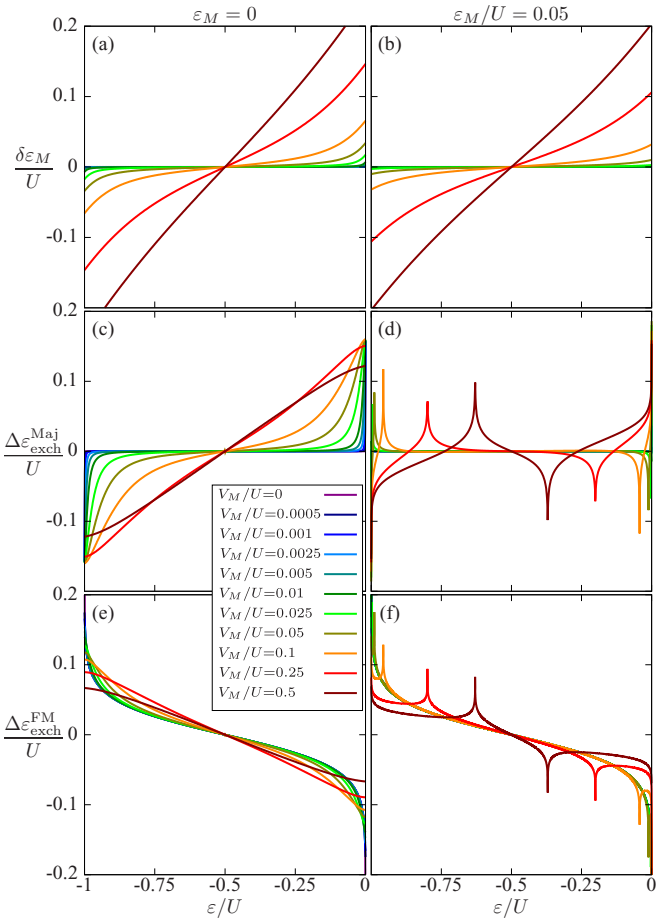

FIG. 2. Different contributions to the ground-state splitting $\Delta\varepsilon^{\rm tot}_{\rm exch}$ as a function of the quantum-dot energy level ε for different couplings to the Majorana wire V_M. The other parameters are $U = 5\Gamma$, $\Gamma = 0.015$ in units of band half-width, $p = 0.5$, and $\varepsilon_M = 0$ (left panel) or $\varepsilon_M = 0.05U$ (right panel). The first row presents the splitting for an isolated Majorana quantum-dot system, $\delta\varepsilon_M$, the second row shows the splitting due to the interaction with nonmagnetic leads, $\Delta\varepsilon^{\rm Maj}_{\rm exch}$, while the third row presents the contribution coming from finite spin polarization of the leads. Note that the curves in the right column overlap for small values of V_M.

with $x_{\Uparrow *} = \varepsilon/2 + U/2 - \varepsilon_M$ and $x_{\Downarrow *} = \varepsilon/2 + \varepsilon_M$. The corresponding splitting of those excited states, denoted by $\delta\varepsilon^*_M$, differs from $\delta\varepsilon_M$ given by Eq. (7) only in the signs of ε_M. In particular, $\delta\varepsilon^*_M = \delta\varepsilon_M$ for $\varepsilon_M = 0$, and $\delta\varepsilon^*_M \approx \delta\varepsilon_M$ for relatively small ε_M.

C. The exchange field

Now we move to the discussion of the full system. In general, the coupling of a QD to metallic leads causes renormalization of its energy levels. In the absence of coupling to Majorana wire, this renormalization results in the spin-splitting of the dot level only in the presence of ferromagnetic leads. Such splitting is then referred to as the ferromagnet-induced exchange field, $\Delta\varepsilon^{\rm FM}_{\rm exch}$ [30,32,35,37,38]. However, in the case of attached Majorana wire, nonmagnetic leads can also cause spin-dependent renormalization, which can be understood as a renormalization of the splitting, $\delta\varepsilon_M$. We denote it by $\Delta\varepsilon^{\rm Maj}_{\rm exch}$. Consequently, the total effective splitting of the ground state can be written in the form

$$\Delta\varepsilon^{\rm tot}_{\rm exch} \equiv \tilde{\varepsilon}_{\Uparrow} - \tilde{\varepsilon}_{\Downarrow} = \delta\varepsilon_M + \Delta\varepsilon^{\rm Maj}_{\rm exch} + \Delta\varepsilon^{\rm FM}_{\rm exch}, \tag{11}$$

where $\tilde{\varepsilon}_{\Uparrow}$ and $\tilde{\varepsilon}_{\Downarrow}$ denote the respective renormalized spin-resolved energy levels of the dot. The splitting caused by the coupling to Majorana wire, renormalized by the interaction with metallic leads, will be denoted by $\Delta\varepsilon_M \equiv \delta\varepsilon_M + \Delta\varepsilon^{\rm Maj}_{\rm exch}$.

For small detunings from the particle-hole symmetry point, small V_M, and $T = 0$, one can expect the FM-induced exchange field to be of the same order as in the single quantum dots coupled to ferromagnetic leads [30],

$$\Delta\varepsilon^{\rm FM}_{\rm exch} \approx -\frac{8p\Gamma}{\pi U}\left(\varepsilon + \frac{U}{2}\right), \tag{12}$$

up to terms linear in $(\varepsilon + U/2)$. On the other hand, neglecting $\Delta\varepsilon^{\rm Maj}_{\rm exch}$, the splitting caused by the coupling to the Majorana wire can be approximated by Eq. (8). Thus, the two splittings are expected to possess different signs. In particular, they can be tuned to compensate for each other.

To get an intuitive understanding of the transport behavior and the interplay between different contributions to the exchange field, we estimate the spin-dependent renormalization of the quantum-dot levels by treating $H_{\rm Tun}$ as a perturbation. In the second order with respect to $V_{r\sigma}$ (first order in Γ_σ), the correction to the energy E_χ of the $H_{\rm DM}$ eigenstate $|\chi\rangle$ can be written as [41]

$$\delta E_\chi = \sum_{\chi'\sigma} \frac{\Gamma}{\pi}(1 + \sigma p)[\Phi(E_{\chi'} - E_\chi)|\langle\chi'|d_\sigma|\chi\rangle|^2 + \Phi(E_\chi - E_{\chi'})|\langle\chi'|d^\dagger_\sigma|\chi\rangle|^2], \tag{13}$$

where the summation over χ' runs through all the $H_{\rm DM}$ eigenstates except for $|\chi\rangle$. The function $\Phi(\varepsilon)$ is given by $\Phi(\varepsilon) = \int d\omega f(\omega)/(\omega - \varepsilon)$, which after using a Lorentzian cutoff can be expressed in terms of the digamma function $\Psi(\varepsilon)$ as

$$\Phi(\varepsilon) = {\rm Re}\left[\Psi\left(\frac{1}{2} + i\frac{\varepsilon}{2\pi T}\right)\right] - \ln\left(\frac{W}{2\pi T}\right). \tag{14}$$

The second term in Eq. (14) comes from the Lorentzian regularization of the finite-temperature integral. In practice, the contributions from such terms cancel out, so that the final expression does not depend on the cutoff parameter W for $W \gg U$. In the numerical calculations, we used $W = 5U$.

The results concerning the nonmagnetic contribution to the exchange field for $\varepsilon_M = 0$ based on Eq. (13) are presented in Fig. 2(c). Clearly, $\Delta\varepsilon^{\rm Maj}_{\rm exch}$ has the same sign and character as $\delta\varepsilon_M$ presented in Fig. 2(a). On the contrary, for $\varepsilon_M = 0.05U$ the signs of $\delta\varepsilon_M$ and $\Delta\varepsilon^{\rm Maj}_{\rm exch}$ may become opposite around the symmetry point [compare Figs. 2(b) and 2(d)]. More precisely, $\Delta\varepsilon^{\rm Maj}_{\rm exch}$ as a function of ε exhibits sharp peaks (divergences at $T \to 0$), which occur at the degeneracy points between the states $|\Downarrow\rangle$ and $|\Uparrow^*\rangle$ (for $\varepsilon > -U/2$) or the states $|\Uparrow\rangle$ and $|\Downarrow^*\rangle$ (for $\varepsilon > -U/2$). For $\varepsilon_M = 0$ these peaks are not present, because for all values of V_M the degeneracy point corresponds to $\varepsilon = -U/2$, where $\Delta\varepsilon^{\rm Maj}_{\rm exch} = 0$ due to symmetry.

Importantly, the perturbative results near the degeneracy points need to be treated with particular care since to describe

the renormalization properly one would need to include higher-order terms. By presenting it, we only intend to demonstrate the mechanism that can lead to the sign change of $\Delta\varepsilon_{\rm exch}^{\rm Maj}$ for certain $\varepsilon \neq -U/2$. This will be clearly reflected in the transport properties obtained with nonperturbative NRG calculations presented and discussed in the next section. Finally, we would also like to note a strong dependence of the magnitude of $\Delta\varepsilon_{\rm exch}^{\rm Maj}$ on V_M, both for vanishing and finite ε_M.

The contribution to the exchange field coming from the spin polarization of the leads for different values of V_M is plotted in Figs. 2(e) and 2(f) for $\varepsilon_M = 0$ and $0.05U$, respectively. As in the case of $\Delta\varepsilon_{\rm exch}^{\rm Maj}$, for $\varepsilon_M = 0$, $\Delta\varepsilon_{\rm exch}^{\rm FM}$ behaves monotonically as a function of ε. It has, however, the opposite sign. One can also see that $\Delta\varepsilon_{\rm exch}^{\rm FM}$ depends only relatively weakly on V_M, so the latter can be used for tuning the system toward the compensation $\Delta\varepsilon_M + \Delta\varepsilon_{\rm exch}^{\rm FM} = 0$. A similar situation holds for finite ε_M. The peaks corresponding to the degeneracy points occur, but the sign of $\Delta\varepsilon_{\rm exch}^{\rm FM}$ near the symmetry point remains unchanged [see Fig. 2(f)]. Thus, in this case compensation of $\Delta\varepsilon_{\rm exch}^{\rm tot}$ by fine-tuning the parameters should be possible.

We note that a more intuitive understanding of the fact that the two splittings have opposite sign can be obtained by inspecting the coupling strengths to spin-up and spin-down dot levels. In the case of a QD-TS system, only the spin-down level is coupled to the topological superconductor. On the other hand, although both dot levels are coupled to ferromagnetic leads, the spin-up coupling is determined by the majority-spin subband and is thus larger than the spin-down coupling. This difference in coupling strengths results in opposite signs of the two induced spin splittings, and in fact it gives rise to their competing nature.

III. NUMERICAL RESULTS AND DISCUSSION

To grasp all the subtle effects resulting from the many-body electronic correlations in the linear-response regime, we use the numerical renormalization group (NRG) method [40,42,43]. In the NRG, the leads are modeled by a semi-infinite chain with exponentially decreasing hopping amplitudes, the zeroth site of which couples to the quantum dot-Majorana wire subsystem. Such a Hamiltonian can be solved in an iterative fashion by exploiting the Z_2 and $U(1)$ symmetries. With the aid of the NRG, we determine the dot-level spectral function $A_\sigma(\omega) = -(1/\pi){\rm Im}\langle\langle d_\sigma | d_\sigma^\dagger\rangle\rangle_\omega^R$, where $\langle\langle d_\sigma | d_\sigma^\dagger\rangle\rangle_\omega^R$ is the Fourier transform of the corresponding retarded Green's function. The relevant correlation functions are calculated using the complete many-body eigenbasis of the NRG Hamiltonian [43–45]. Assuming that the topological superconductor is floating and the voltage drop is applied symmetrically between the ferromagnets, one can determine the linear-response conductance between the left and right leads from the following formula [46]:

$$G = \frac{e^2}{h}\pi\Gamma\int d\omega\left(-\frac{\partial f}{\partial\omega}\right)[(1+p)A_\uparrow(\omega) + (1-p)A_\downarrow(\omega)],$$

where f denotes the Fermi-Dirac distribution function.

As follows from the discussion in the previous section, the spin-resolved transport properties will be determined by the interplay between the Kondo temperature T_K, the exchange field $\Delta\varepsilon_{\rm exch}^{\rm FM}$, and the splitting $\Delta\varepsilon_M$ caused by the coupling to Majorana wire, $\Gamma_M = \pi\rho_{\rm QD}V_M^2$, where $\rho_{\rm QD}$ is the density of states of the dot. In the Kondo regime, the latter can be estimated from $\Gamma_M \approx 2V_M^2/\Gamma$ [15]. On the other hand, the Kondo temperature in the case of $V_M = 0$ and $p = 0$ for assumed parameters ($U = 0.2$ and $\Gamma = 0.015$ in units of band half-width [42]) and $\varepsilon = -U/2$ is approximately equal to [47] $T_K^0/U \approx 0.001$.

In the following, we first study the spectral properties of the system and then analyze the conductance, together with its spin polarization, in the full parameter space for arbitrary temperatures and couplings to the topological superconductor. For comparison, we present and discuss the transport characteristics in the case of both nonmagnetic (NM) and ferromagnetic (FM) leads.

A. Spectral properties

The zero-temperature normalized spectral function, $\mathcal{A} \equiv \sum_\sigma \pi\Gamma_\sigma A_\sigma(\omega)$, in the case of FM leads with spin polarization $p = 0.5$ is shown in Fig. 3 for different values of the dot-level position ε and coupling to the topological superconductor V_M. The left column corresponds to the case of the infinitely long Majorana wire ($\varepsilon_M = 0$), while the right column shows the results for a finite-length nanowire, assuming $\varepsilon_M/U = 0.05$. To resolve different energy scales playing an important role in the transport properties, the spectral function is plotted on a logarithmic scale.

Let us start the discussion with the case of $\varepsilon_M = 0$. When the system is tuned to the particle-hole symmetry point, $\varepsilon = -U/2$, both $\Delta\varepsilon_{\rm exch}^{\rm FM}$ and $\Delta\varepsilon_M$ are then equal to zero. In this situation, the system behaves as if coupled to nonmagnetic leads with slightly modified Kondo temperature [15,20]. When $V_M = 0$, the system exhibits the Kondo effect with $\mathcal{A}_{\rm FM} = 2$ for $\omega \to 0$. On the other hand, for finite V_M, the normalized spectral function in the spin-down channel for $\omega \to 0$ equals $\pi\Gamma_\downarrow A_\downarrow(0) = 1/2$, as a consequence of the Kondo effect and the destructive interference caused by the interaction with the Majorana zero-energy mode [12,15]. For the spin-up channel, which is not directly coupled to the topological superconductor, one simply has $\pi\Gamma_\uparrow A_\uparrow(0) = 1$ due to the Kondo effect. As a consequence, one then finds $\mathcal{A}_{\rm FM} = 3/2$ for $\omega \to 0$ [see Fig. 3(a)]. The normalized spectral function exhibits a plateau of width proportional to T_K as long as $\Gamma_M \gtrsim T_K$, otherwise $\mathcal{A}_{\rm FM}$ exhibits a local maximum with $\mathcal{A}_{\rm FM} \to 2$ for $\Gamma_M \lesssim |\omega| \lesssim T_K$; see, e.g., the curve for $V_M/U = 0.0005$ in Fig. 3(a). When $\Gamma_M \gtrsim T_K$, a further increase of V_M leads in turn to an enhancement of the Kondo temperature, which is clearly visible as a broadening of the Kondo peak in $\mathcal{A}_{\rm FM}$ (see Fig. 3).

Out of the particle-hole symmetry point, the behavior of the spectral function is definitely more complex. First of all, we recall that there are now more energy scales determining the transport properties, because both the exchange field and the splitting caused by the coupling to Majorana wire are finite once $\varepsilon \neq -U/2$. Moreover, in the considered parameter range, $\Delta\varepsilon_{\rm exch}^{\rm FM}$ is typically much larger (in terms of the absolute value) than $\Delta\varepsilon_M$, due to $\Gamma > \Gamma_M$. This situation is presented in Fig. 3(c), which shows the spectral function calculated for $\varepsilon = -0.49U$. For $V_M = 0$, $\mathcal{A}_{\rm FM}(0)$ is suppressed due to the

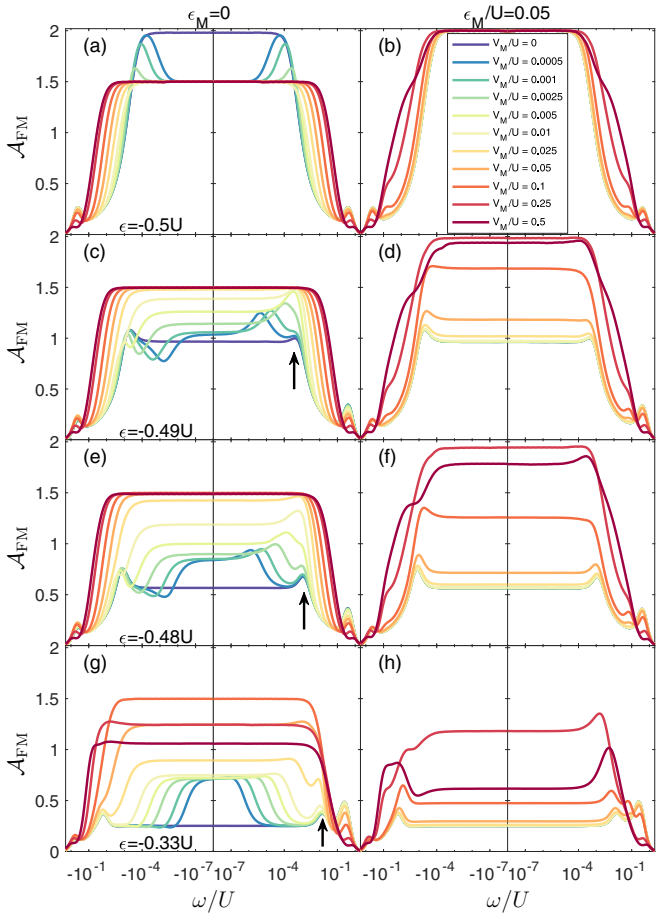

FIG. 3. The zero-temperature normalized spectral function, $\mathcal{A} \equiv \sum_\sigma \pi\Gamma_\sigma A_\sigma(\omega)$, calculated for different couplings to Majorana wire V_M, as indicated. The left (right) column corresponds to the case of $\varepsilon_M = 0$ ($\varepsilon_M/U = 0.05$), while the consecutive rows show the results for $\varepsilon = -0.5U$, $\varepsilon = -0.49U$, $\varepsilon = -0.48U$, and $\varepsilon = -0.33U$, respectively. The vertical arrows indicate the magnitude of the exchange field. The curves for finite ε_M start to overlap when $V_M/U \lesssim 0.005$. The other parameters are the same as in Fig. 2.

spin-splitting of the dot level by $\Delta\varepsilon^{\rm FM}_{\rm exch}$. Note that in this case $|\Delta\varepsilon^{\rm FM}_{\rm exch}| \approx T_K^0$; see the vertical arrow in Fig. 3(c).

When V_M increases, a small peak (dip) occurs in the spectral function for $\omega \approx \Gamma_M$ ($\omega \approx -\Gamma_M$). Moreover, once $\Gamma_M \gtrsim |\Delta\varepsilon^{\rm FM}_{\rm exch}|$, a plateau in $\mathcal{A}_{\rm FM}$ develops with $\mathcal{A}_{\rm FM} = 3/2$ [see Fig. 3(c)]. This results from the fact that increasing V_M leads to an enhancement of T_K and, additionally, to an increase of $\Delta\varepsilon_M$. Consequently, when $T_K \gtrsim |\Delta\varepsilon^{\rm tot}_{\rm exch}|$, the exchange-field-generated splitting does not play an important role, and the spectral function behaves similarly to the case of $\varepsilon = -U/2$ for $\Gamma_M \gtrsim T_K$.

For larger detunings, the above-described effects become even more pronounced. The suppression of $\mathcal{A}_{\rm FM}$ at $\omega = 0$ due to the exchange field gets enhanced. Because of that, larger coupling to Majorana wire is necessary to restore the Kondo peak of height $\mathcal{A}_{\rm FM} = 3/2$. Furthermore, it can be seen for $\varepsilon/U = -0.33$ that the dependence of the spectral function for $\omega = 0$ is not monotonic when changing V_M. Increasing the coupling to the topological superconductor leads to an enhancement of $\mathcal{A}_{\rm FM}$ to the value of 3/2 [see the curve for $V_M/U = 0.1$ in Fig. 3(g)], however larger values of V_M bring about the suppression of the spectral function again. This is associated with an increase of $\Delta\varepsilon_M$, such that $|\Delta\varepsilon_M| > |\Delta\varepsilon^{\rm FM}_{\rm exch}|$.

When the length of the topological superconductor wire is smaller than the corresponding superconducting phase coherence length, a considerable overlap between the two Majorana zero-energy modes located at the ends of the wire is present [9]. The normalized spectral function of the dot level calculated for different V_M and ε in the case of $\varepsilon_M/U = 0.05$ is presented in the right column of Fig. 3. As can be seen for $\varepsilon = -U/2$, only relatively large coupling to the topological superconductor affects the behavior of the spectral function, and its influence is rather qualitative, as it only increases T_K [see Fig. 3(b)]. This is because the splitting of Majorana zero-energy modes, described by γ_1 and γ_2 operators, blocks the interference effects, and the Kondo effect is not influenced by the coupling Γ_M [15]. Consequently, in the case of $\varepsilon = -U/2$ the Kondo peak is present for any value of V_M [see Fig. 3(b)]. When the dot level is detuned from the particle-hole symmetry, the situation changes since the spectral function for $V_M = 0$ is already suppressed by the exchange field. Now, with increasing V_M, T_K increases and the Kondo effect can be restored for large V_M such that $T_K \gtrsim |\Delta\varepsilon^{\rm tot}_{\rm exch}|$; see the case of $\varepsilon/U = -0.49$ shown in Fig. 3(d). This restoration happens only partially for larger detunings since then the exchange field is much larger and it is not possible to fully reinstate the Kondo peak [see Figs. 3(f) and 3(h)].

The interplay between the respective energy scales can be nicely revealed by studying the density plots of the normalized spectral function as a function of energy ω and dot-level position calculated for different values of V_M. The corresponding plots in the case of $\varepsilon_M = 0$ are presented in Fig. 4. The right column shows the spectral function for ferromagnetic contacts, $\mathcal{A}_{\rm FM}$, while the left column displays the spectral function for nonmagnetic leads, $\mathcal{A}_{\rm NM}$, for comparison. In the case of nonmagnetic leads, for $V_M = 0$, the spectral function exhibits the Kondo resonance in the singly occupied regime, $-U \ll \varepsilon \ll \Gamma$, with $\mathcal{A}_{\rm NM} = 2$ at the Fermi level [see Fig. 4(a)]. When the coupling to the topological superconductor increases, the maximum value of $\mathcal{A}_{\rm NM}$ drops to 3/2 in the Kondo regime and 1/2 in the even occupation dot regime. This is due to the fact that the interference with the Majorana zero-energy mode results in $\pi\Gamma A_\downarrow(0) = 1/2$ irrespective of ε, while $A_\uparrow(0)$ shows the Kondo peak in the singly occupied dot regime and is suppressed out of the Kondo regime, since then only elastic cotunneling processes are possible. Note also that with increasing V_M, the width of the Kondo plateau decreases; see, e.g., the case of $V_M/U = 0.25$ in Fig. 4(i).

In the case of ferromagnetic leads, the splitting of the Kondo resonance is clearly visible [see Fig. 4(b)]. When increasing V_M, the characteristic x-like split-Kondo-resonance feature becomes modified. The coupling to the Majorana mode increases the value of the spin-down spectral function at the Fermi level to $1/(2\pi\Gamma_\downarrow)$, while the spin-up component is suppressed by the exchange field. As a result, a narrow resonance at $\omega = 0$ in the whole range of ε develops with increasing V_M [see Figs. 4(d) and 4(f)]. In addition, finite V_M also modifies the side peaks of the split Kondo resonance. This is associated with (i) the coupling Γ_M, which leads to

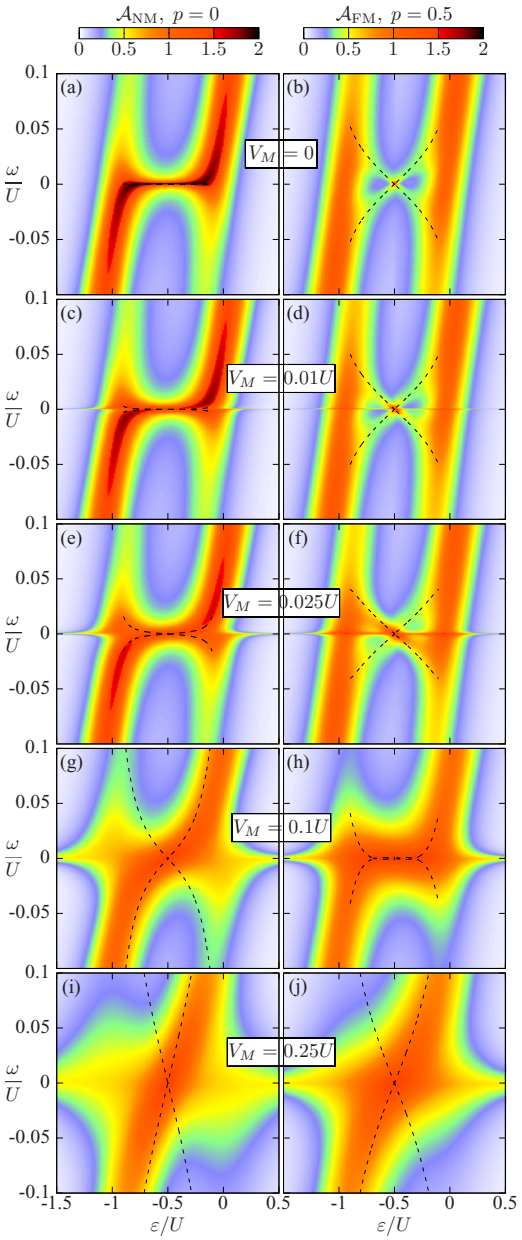

FIG. 4. The energy and dot-level position dependence of the zero-temperature normalized spectral function in the case of NM, $\mathcal{A}_{\rm NM}$ (left column), and FM, $\mathcal{A}_{\rm FM}$ (right column), leads calculated for different strengths of coupling to Majorana wire, as indicated. The parameters are the same as in Fig. 3. This figure corresponds to the case of infinite Majorana wire, $\varepsilon_M = 0$. The dashed lines indicate the splitting of the ground state, $\Delta\varepsilon^{\rm tot}_{\rm exch}$, estimated according to Eq. (11).

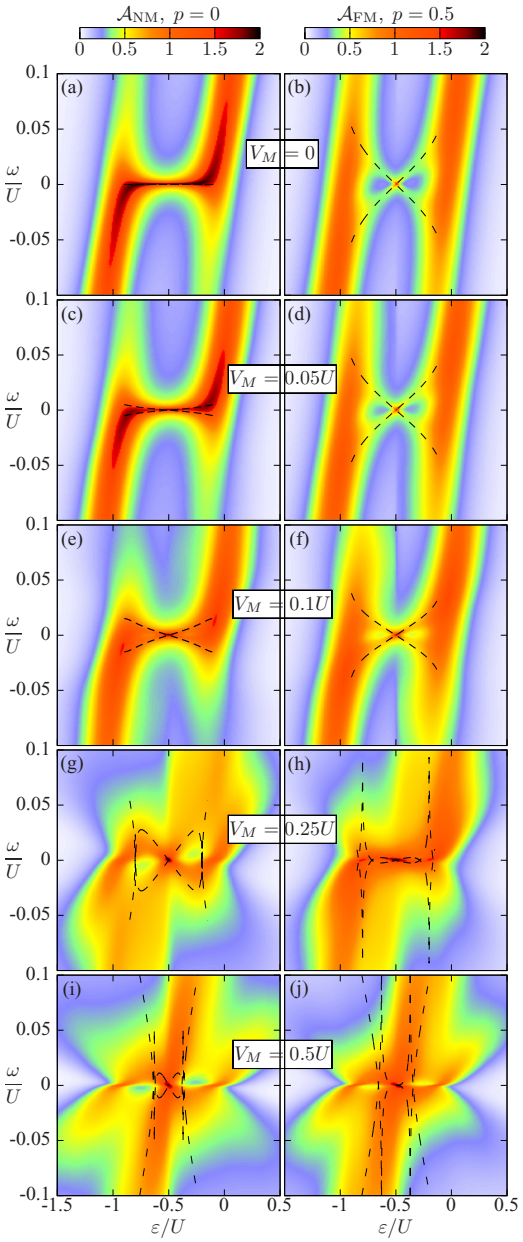

FIG. 5. The same as in Fig. 4 calculated in the case of $\varepsilon_M/U = 0.05$. The dashed lines indicate the splitting of the ground state, as described by Eq. (11).

an enhancement of T_K, and (ii) $\Delta\varepsilon_M$, which tends to decrease the splitting caused by the exchange field (recall that these two splittings have different signs). For $V_M/U \gtrsim 0.1$, the exchange-field-induced splitting is already suppressed and the spectral function displays a pronounced Kondo resonance with $\mathcal{A}_{\rm FM} = 3/2$ [see Figs. 4(h) and 4(j)].

The density plots for the normalized spectral function in the case when the overlap between the two Majorana fermions is finite are shown in Fig. 5. As can be seen, in the case of both nonmagnetic and ferromagnetic leads, the coupling to the topological superconductor starts modifying the behavior of the spectral function for relatively large couplings, $V_M/U \gtrsim 0.05$. In the case of nonmagnetic leads, a pronounced splitting of the Kondo resonance develops. This is associated with $\Delta\varepsilon_M$, which now can surpass the Kondo temperature. Note that at the particle-hole symmetry point, $\mathcal{A}_{\rm NM} = 2$ for all values of V_M considered since at this point $\Delta\varepsilon_M = 0$; see the left column of Fig. 5. In the case of ferromagnetic leads, one can notice the interplay of the splittings caused by $\Delta\varepsilon^{\rm FM}_{\rm exch}$ and $\Delta\varepsilon_M$; see the right column of Fig. 5. When the coupling to the topological superconductor increases, the splitting due to $\Delta\varepsilon^{\rm FM}_{\rm exch}$ starts decreasing until it becomes roughly compensated for $V_M/U = 0.25$. In turn, a further increase of V_M generates the splitting again, due to $|\Delta\varepsilon_M| > |\Delta\varepsilon^{\rm FM}_{\rm exch}|$ [see Fig. 5(j)].

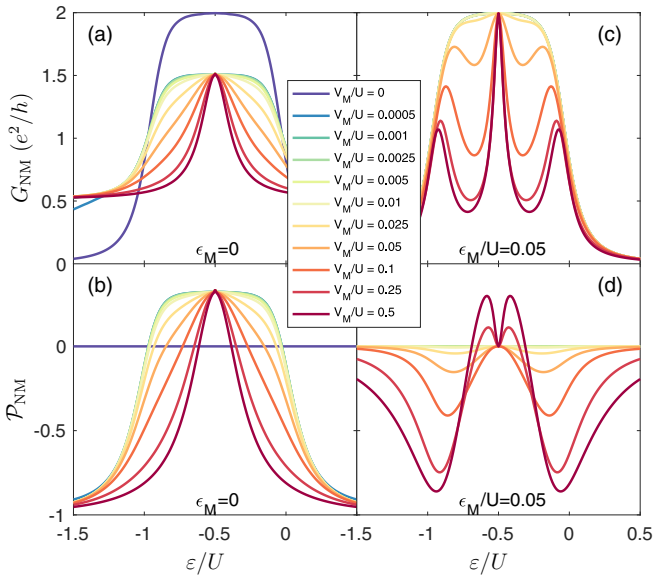

FIG. 6. The zero-temperature linear conductance (first row) and the corresponding conductance spin polarization (second row) as a function of the dot-level position calculated in the case of nonmagnetic leads ($p = 0$) for different couplings to topological superconductor V_M. The left (right) column corresponds to the case of $\varepsilon_M = 0$ ($\varepsilon_M/U = 0.05$). Note that the curves for finite ε_M start to overlap when $V_M/U \lesssim 0.01$. The other parameters are the same as in Fig. 3.

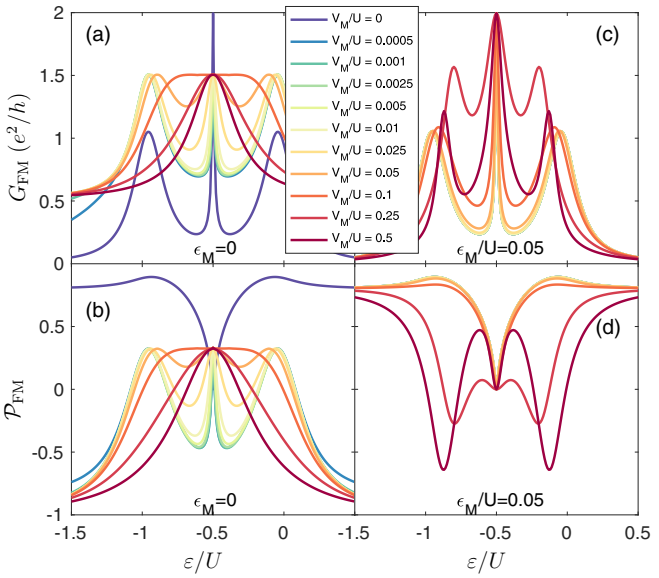

FIG. 7. The same as in Fig. 6 calculated in the case of ferromagnetic leads with $p = 0.5$. For $\varepsilon_M/U = 0.05$, the curves overlap when $V_M/U \lesssim 0.01$.

B. Linear conductance and spin polarization

The different behavior of the spectral function is clearly revealed in the linear-response conductance, the behavior of which is presented and discussed in this section. First, we analyze the conductance as a function of dot-level position for different couplings V_M and different overlaps between Majorana zero-energy modes ε_M, and then we study the temperature dependence of G. In addition, we also discuss the behavior of the spin polarization of conductance $\mathcal{P}$, which is defined as $\mathcal{P} = (G_\uparrow - G_\downarrow)/(G_\uparrow + G_\downarrow)$, where G_σ is the linear conductance in spin channel σ.

1. Dot-level position dependence

The dot-level position dependence of the linear conductance $G_{\rm NM}$ in the case of nonmagnetic leads is shown in the first row of Fig. 6, while the second row presents the corresponding spin polarization $\mathcal{P}_{\rm NM}$. The left (right) column presents the case of $\varepsilon_M = 0$ ($\varepsilon_M/U = 0.05$). In the Kondo regime, the interference effects with the Majorana zero-energy mode in the case of $\varepsilon_M = 0$ immediately lead to a decrease of $G_{\rm NM}$ from $2e^2/h$ to $3e^2/2h$. On the other hand, out of the Kondo regime, the conductance reaches a value of $e^2/2h$. The effect of increasing V_M is seen as a gradual narrowing of the Kondo plateau, until a single peak remains for large values of V_M [see Fig. 6(a)]. The conductance spin polarization in the Kondo regime takes a constant value of $\mathcal{P}_{\rm NM} = 1/3$ because $G_\uparrow = 2G_\downarrow$, while in the even-occupation dot regime it reaches $\mathcal{P}_{\rm NM} = -1$ due to $G_\downarrow \gg G_\uparrow$ [see Fig. 6(b)]. This is direct evidence that transport results mainly from the spin-down channel, in which $G_\downarrow = e^2/2h$.

In the case of finite ε_M, the behavior of conductance is completely different. In fact, it resembles that of quantum dots with ferromagnetic contacts [38]. This is not surprising because the coupling to Majorana wire results in spin-splitting of the dot level, which grows upon increasing the detuning from the particle-hole symmetry point, while for $\varepsilon = -U/2$, $\Delta\varepsilon_M = 0$. This can be clearly seen in Fig. 6(c): when V_M grows, the conductance develops two local minima for ε around $\varepsilon = -U/2$, while at the particle-hole symmetry point $G_{\rm NM} = 2e^2/h$. Note also that due to large ε_M, the conductance in the even dot occupation regime is also suppressed. The behavior of the conductance is reflected in the spin polarization, which is mainly negative except for the values of ε around $\varepsilon = -U/2$ for large V_M [see Fig. 6(d)]. Moreover, now the spin polarization is determined only by finite spin splitting $\Delta\varepsilon_M$, and because of that, $\mathcal{P}_{\rm NM} = 0$ at the particle-hole symmetry point since $G_\uparrow = G_\downarrow = e^2/h$.

The linear conductance and spin polarization as a function of ε in the case of ferromagnetic leads are shown in Fig. 7. Let us first discuss the case of $\varepsilon_M = 0$. In the absence of coupling to the topological superconductor, $G_{\rm FM}$ is generally suppressed except for resonances and $\varepsilon = -U/2$. At the particle-hole symmetry point, $\Delta\varepsilon^{\rm tot}_{\rm exch} = 0$ and $G_{\rm FM} = 2e^2/h$ due to the Kondo effect. When the coupling to Majorana wire becomes finite, a general observation is that $G_{\rm FM}$ becomes enhanced by a factor of $e^2/2h$ (this is the constant contribution coming from the spin-down channel), apart from $\varepsilon = -U/2$, where the conductance is suppressed by the same amount. For larger couplings to the topological superconductor, the exchange-field-induced suppression of $G_{\rm FM}$ becomes diminished and the conductance eventually exhibits a plateau for $V_M/U \approx 0.1$, which turns into a peak for larger V_M [see Fig. 7(a)]. The spin polarization of the conductance also changes drastically when the coupling to Majorana wire is finite. In the case of $V_M = 0$, $\mathcal{P}_{\rm FM} = 0$ for $\varepsilon = -U/2$ and then grows when detuning the

dot level to reach the value of $\mathcal{P}_{\rm FM} = 2p/(1+p^2)$ in the even dot occupation regime [38]. When $V_M > 0$, $\mathcal{P}_{\rm FM}$ equals -1 out of the Kondo regime and reaches $1/3$ in the Kondo regime for such values of V_M that the Kondo plateau is restored. On the other hand, for smaller couplings to Majorana wire, $\mathcal{P}_{\rm FM}$ first drops and becomes negative when detuning the level from the particle-hole symmetry point to reach $\mathcal{P}_{\rm FM} = 1/3$ at resonance, and then decreases again to -1 for $\varepsilon \ll -U$ or $\varepsilon \gg \Gamma$ [see Fig. 7(b)].

The dot-level dependence of $G_{\rm FM}$ in the case of finite ε_M is presented in Fig. 7(c). For low values of V_M, the ε dependence of conductance is the same as in the absence of the topological superconductor. This dependence starts changing when $V_M/U \gtrsim 0.05$. With increasing V_M, the conductance first becomes enhanced for $V_M/U = 0.25$, but then it drops again for larger V_M [see Fig. 7(c)]. As was already discussed in the previous section, this is associated with the interplay of the two splittings. In fact, by fine-tuning V_M, one could compensate for the ferromagnetic-lead-induced splitting and restore the Kondo plateau completely. The associated dependence of the spin polarization is shown in Fig. 7(d). It can be seen that $\mathcal{P}_{\rm FM}$ is generally positive except for resonances and large values of V_M, where $\mathcal{P}_{\rm FM}$ can change sign. This indicates that the spin-up (majority) channel is giving the dominant contribution to the conductance. Note that it is just opposite to the case of $\varepsilon_M = 0$ [cf. Figs. 6(d) and 7(d)].

Because in reality the length of the topological superconductor wire is always finite, which results in a finite overlap ε_M between the two Majorana zero-energy modes, we now study the dependence of the conductance and the spin polarization on both ε and ε_M. Figure 8 displays the ε and ε_M dependence of the conductance for different values of V_M, where the left (right) column corresponds to the nonmagnetic (ferromagnetic) lead case. When the coupling to Majorana wire is relatively weak, a finite overlap between the two Majorana fermions blocks the interference effects, and the half-fermionic nature of the Majorana mode, leading to a fractional value of conductance, is not revealed. In this case, the dot-level dependence of the linear conductance resembles that in the case of $V_M = 0$. For larger values of the coupling V_M, the conductance starts depending on ε_M (see Fig. 8). One can observe that for small values of the overlap ε_M, the conductance in the nonmagnetic case reveals the features discussed earlier. $G_{\rm NM}$ is suppressed in the Kondo regime due to the spin-splitting $\Delta\varepsilon_M$, apart from $\varepsilon = -U/2$, where $G_{\rm NM}$ exhibits a peak. On the other hand, in the even occupation dot regime, $G_{\rm NM} = e^2/2h$. When the value of ε_M increases, these features start gradually changing: the Kondo plateau develops in the Coulomb blockade regime with $G_{\rm NM} = 2e^2/h$, while the conductance in the even dot occupation regime becomes suppressed for large ε_M. Note that if the coupling to topological wire is sufficiently strong, the behavior of $G_{\rm NM}$ depends only weakly on ε_M. The suppression of the Kondo resonance except for $\varepsilon = -U/2$ is still present, while the main change can be seen for the empty and doubly occupied dot regimes, where the universal value of $G_{\rm NM} = e^2/2h$ is no longer retained and $G_{\rm NM}$ decreases with ε_M.

When the leads are ferromagnetic, the conductance out of the Kondo regime is generally suppressed for all values of ε_M and V_M considered; see the right column of Fig. 8.

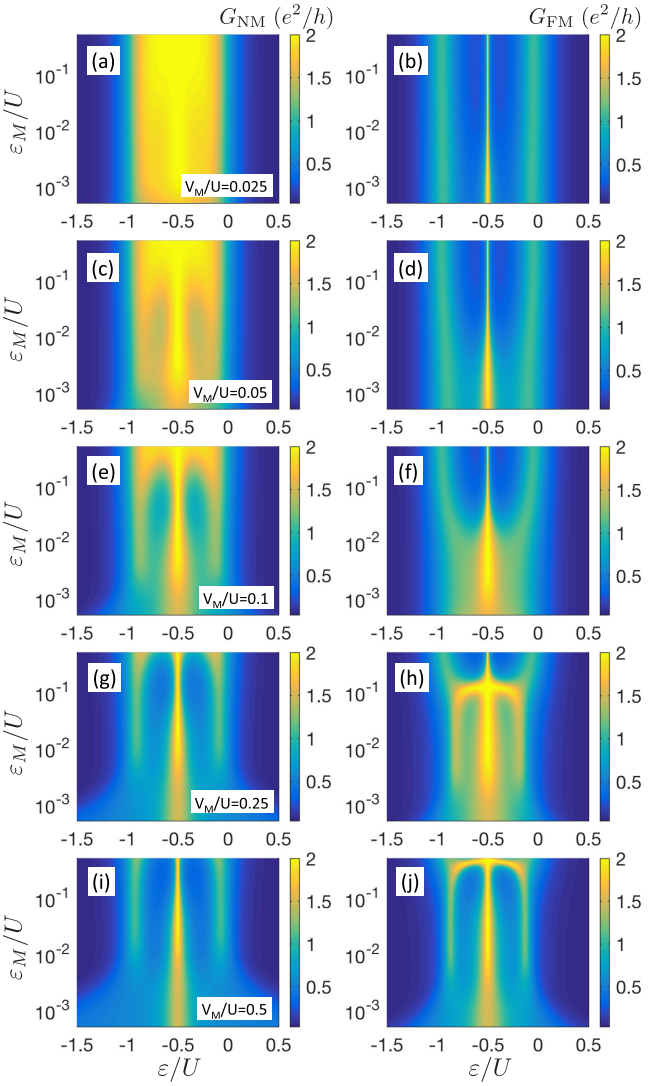

FIG. 8. The linear conductance as a function of the dot-level position ε and the overlap between the two Majorana fermions ε_M calculated for different couplings V_M, as indicated. The left (right) column corresponds to the nonmagnetic (ferromagnetic) lead case. The parameters are the same as in Fig. 3.

Moreover, the suppression of $G_{\rm FM}$ in the Kondo regime due to the spin splitting caused by the ferromagnetic-contact-induced exchange field and the splitting induced by the coupling to the topological superconductor also takes place. In fact, the interplay of those splittings and their competing nature can lead to the restoration of the Kondo plateau for some parameters. This can be clearly seen in Fig. 8(h). We note that the Kondo effect for $\varepsilon = -U/2$ is present for all values of ε_M and V_M, since then $\Delta\varepsilon^{\rm FM}_{\rm exch} = \Delta\varepsilon_M = 0$.

The ε and ε_M dependence of the associated spin polarization in the case of both nonmagnetic and ferromagnetic leads is shown in Fig. 9. Let us first discuss $\mathcal{P}$ in the nonmagnetic case. One can see that with increasing V_M, the absolute value of the spin polarization increases. This is quite natural since for larger couplings the spin splitting of the dot level triggered by the presence of Majorana modes becomes enhanced, consequently $|\mathcal{P}_{\rm NM}|$ increases; see the left column of Fig. 9.

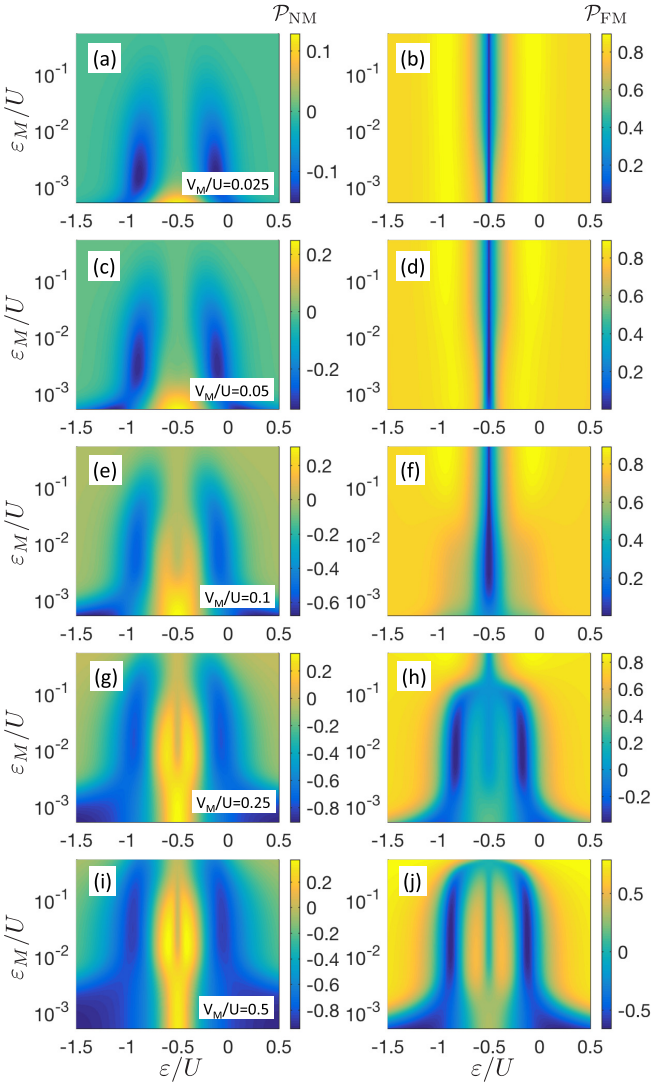

FIG. 9. The spin polarization of the conductance in the case of nonmagnetic ($\mathcal{P}_{\rm NM}$, left column) and ferromagnetic ($\mathcal{P}_{\rm FM}$, right column) leads as a function of the dot-level position and the overlap between the two Majorana modes calculated for different couplings V_M. The parameters are the same as in Fig. 3.

For $V_M/U \gtrsim 0.1$, an extra feature with positive $\mathcal{P}_{\rm NM}$ develops in the Coulomb blockade regime. This happens when the conductance suppression due to the spin-splitting $\Delta\varepsilon_M$ is most effective [see Figs. 9(g) and 9(i)]. On the other hand, in the case of ferromagnetic leads, the spin polarization is generally positive when the Majorana-related effects are relatively weak. Their presence is revealed, among others, as a gradual sign change of $\mathcal{P}_{\rm FM}$. This indicates that the spin-down channel becomes dominant due to the Majorana-induced interference effects; see the right column of Fig. 9.

2. *Temperature dependence*

We turn now to an analysis of the temperature dependence of the linear conductance in all the considered cases. Figure 10 presents $G_{\rm NM}$ as a function of T calculated for different V_M and two selected values of ε_M and ε. Consider now the case of $\varepsilon_M = 0$. The dependence $G_{\rm NM}(T)$ for $V_M = 0$ presents the

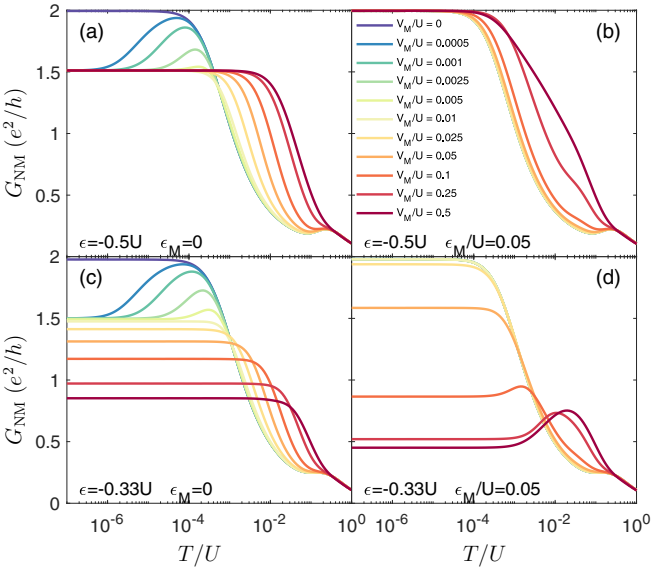

FIG. 10. The temperature dependence of the linear conductance $G_{\rm NM}$ in the case of nonmagnetic leads calculated for different couplings to the Majorana mode V_M, as indicated. The first (second) row shows the results for $\varepsilon = -0.5U$ ($\varepsilon = -0.33U$), while the first (second) column presents the data for $\varepsilon_M = 0$ ($\varepsilon_M/U = 0.05$). Note that in the case of finite ε_M, the curves overlap when $V_M/U \lesssim 0.01$. The other parameters are the same as in Fig. 3.

usual conductance curve with $G_{\rm NM}$ approaching $2e^2/h$ for $T \ll T_K$, with the maximum value slightly lower for ε out of the particle-hole symmetry point. When the coupling to Majorana wire becomes finite, the zero-temperature value of conductance drops to a fractional value of $3e^2/2h$. If $\Gamma_M \lesssim T_K$, then $G_{\rm NM}$ exhibits a local maximum for $\Gamma_M \lesssim T \lesssim T_K$ [see Figs. 10(a) and 10(c)]. When, however, $\Gamma_M \gtrsim T_K$, the conductance equals $3e^2/2h$ for the particle-hole symmetry point and starts decreasing out of this point. This decrease is a direct indication of the splitting $\Delta\varepsilon_M$. We also note that upon raising V_M, the Kondo temperature becomes enhanced.

When the overlap between the two Majorana zero-energy modes is finite, the energy of the Majorana states becomes split. This results in the suppression of interference effects between the dot and the topological superconductor, such that the dot exhibits the usual Kondo effect with $G_{\rm NM} = 2e^2/h$. Only when the coupling V_M becomes sufficiently strong can one observe the influence of this coupling on the transport behavior. In the case of $\varepsilon = -U/2$, it results in an enhancement of T_K [see Fig. 10(b)], while for $\varepsilon/U = -0.33$ the maximum value of conductance becomes suppressed with V_M due to the development of $\Delta\varepsilon_M$ [see Fig. 10(d)].

The temperature dependence in the case of ferromagnetic leads is presented in Fig. 11, with the left (right) column corresponding to the infinite (finite) Majorana wire case. When the dot is tuned to the particle-hole symmetry point, the dependence of $G_{\rm FM}$ on temperature is qualitatively the same as in the nonmagnetic case, irrespective of ε_M. This is because at this point the exchange field does not play any role and the system behaves as if coupled to nonmagnetic leads with slightly modified T_K [see Figs. 11(a) and 11(b)].

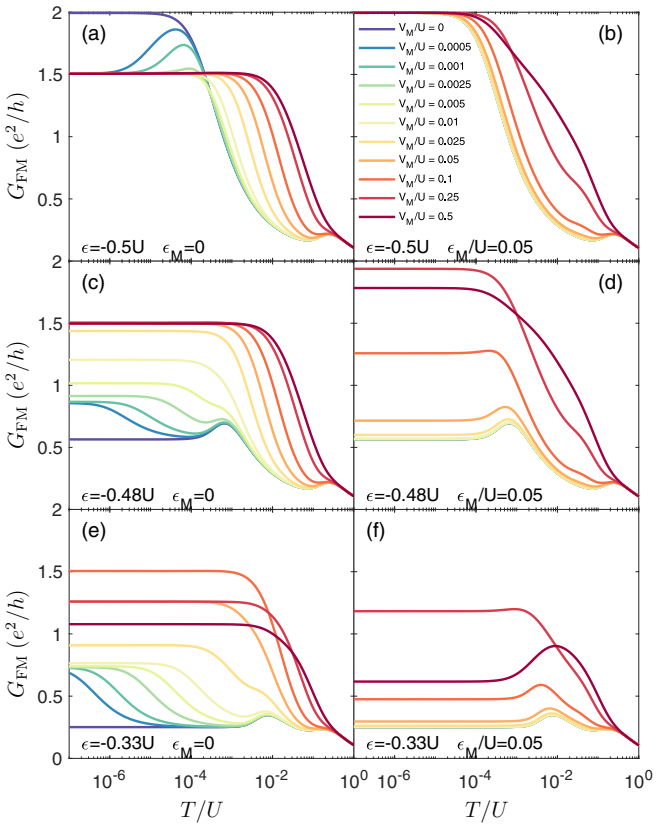

FIG. 11. The temperature dependence of the linear conductance $G_{\rm FM}$ in the case of ferromagnetic leads calculated for different couplings to the Majorana mode V_M, as indicated. The left (right) column corresponds to the case of $\varepsilon_M = 0$ ($\varepsilon_M/U = 0.05$), while the consecutive rows show the data for $\varepsilon = -0.5U$, $-0.48U$, and $-0.33U$, respectively. Note that in the case of finite ε_M, the curves overlap when $V_M/U \lesssim 0.01$. The other parameters are the same as in Fig. 3.

For small detunings from the particle-hole symmetry point [see the second row of Fig. 11, which shows $G_{\rm FM}(T)$ for $\varepsilon = -0.48U$], the exchange field is already larger than T_K and the Kondo effect is suppressed. Enhancing the coupling to the topological superconductor gradually restores the Kondo effect, and the conductance becomes enhanced to $3e^2/2h$ in the case of $\varepsilon_M = 0$ and $2e^2/h$ for finite ε_M. When the detuning from $\varepsilon = -U/2$ is increased, the conductance suppression at low temperatures is even larger. It can also be clearly seen that when the coupling to Majorana wire grows, the conductance becomes enhanced for certain values of V_M, but then it drops again [see Figs. 11(e) and 11(f)]. This is due to the interplay between the two splittings, as discussed in the previous section.

IV. SUMMARY

In this paper, we have analyzed the spin-resolved transport properties of a quantum dot coupled to both nonmagnetic and ferromagnetic leads and additionally attached to topological superconductor wire hosting Majorana zero-energy modes at its ends. The analysis was performed in the linear-response regime with the aid of the numerical renormalization group method. We determined the behavior of the dot-level spectral function, the conductance and its spin polarization on the position of the dot level, the temperature, and the strength of coupling to Majorana wire. Our results revealed that the transport behavior in the case of ferromagnetic leads results from the interplay between the Kondo correlations, exchange-field-induced splitting, and the coupling to the topological superconductor with associated splitting of the dot level. We demonstrated that these two splittings compete, and for some parameters they can counterbalance each other, restoring the Kondo effect. These distinct features of transport properties may serve as another indication of the presence of Majorana zero-energy modes in considered nanoscale devices.

Finally, we note that although we considered a three-terminal device, at equilibrium our system can be mapped to a two-terminal setup, with one ferromagnetic lead having an effective spin polarization. In this regard, the results presented in this paper may be applicable to two-terminal hybrid Majorana devices, the spectral properties of which could be probed with a weakly attached probe, such as a tip of a scanning tunneling microscope.

ACKNOWLEDGMENTS

We acknowledge discussions with C. P. Moca. This work was supported by the National Science Centre in Poland through Project No. DEC-2013/10/E/ST3/00213. Computing time at the Poznań Supercomputing and Networking Center is acknowledged.

[1] M. Z. Hasan and C. L. Kane, Rev. Mod. Phys. **82**, 3045 (2010).
[2] X.-L. Qi and S.-C. Zhang, Rev. Mod. Phys. **83**, 1057 (2011).
[3] A. Y. Kitaev, Ann. Phys. (NY) **303**, 2 (2003).
[4] C. Nayak, S. H. Simon, A. Stern, M. Freedman, and S. Das Sarma, Rev. Mod. Phys. **80**, 1083 (2008).
[5] E. Majorana, Nuovo Cimento **14**, 171 (1937).
[6] V. Mourik, K. Zuo, S. M. Frolov, S. R. Plissard, E. P. A. M. Bakkers, and L. P. Kouwenhoven, Science **336**, 1003 (2012).
[7] M. T. Deng, C. L. Yu, G. Y. Huang, M. Larsson, P. Caro, and H. Q. Xu, Nano Lett. **12**, 6414 (2012).
[8] A. Das, Y. Ronen, Y. Most, Y. Oreg, M. Heiblum, and H. Shtrikman, Nat. Phys. **8**, 887 (2012).
[9] S. M. Albrecht, A. P. Higginbotham, M. Madsen, F. Kuemmeth, T. S. Jespersen, J. Nygard, P. Krogstrup, and C. M. Marcus, Nature (London) **531**, 206 (2016).
[10] K. Flensberg, Phys. Rev. B **82**, 180516 (2010).
[11] A. Golub, I. Kuzmenko, and Y. Avishai, Phys. Rev. Lett. **107**, 176802 (2011).
[12] D. E. Liu and H. U. Baranger, Phys. Rev. B **84**, 201308(R) (2011).
[13] M. Leijnse and K. Flensberg, Phys. Rev. B **84**, 140501(R) (2011).
[14] Y. Cao, P. Wang, G. Xiong, M. Gong, and X.-Q. Li, Phys. Rev. B **86**, 115311 (2012).

[15] M. Lee, J. S. Lim, and R. Lopez, Phys. Rev. B **87**, 241402(R) (2013).
[16] E. Vernek, P. H. Penteado, A. C. Seridonio, and J. C. Egues, Phys. Rev. B **89**, 165314 (2014).
[17] R. Lopez, M. Lee, L. Serra, and J. S. Lim, Phys. Rev. B **89**, 205418 (2014).
[18] M. Leijnse, New J. Phys. **16**, 015029 (2014).
[19] W.-J. Gong, S.-F. Zhang, Z.-C. Li, G. Yi, and Y.-S. Zheng, Phys. Rev. B **89**, 245413 (2014).
[20] M. Cheng, M. Becker, B. Bauer, and R. M. Lutchyn, Phys. Rev. X **4**, 031051 (2014).
[21] D. E. Liu, M. Cheng, and R. M. Lutchyn, Phys. Rev. B **91**, 081405 (2015).
[22] D. A. Ruiz-Tijerina, E. Vernek, L. G. G. V. Dias da Silva, and J. C. Egues, Phys. Rev. B **91**, 115435 (2015).
[23] J. P. Ramos-Andrade, O. Avalos-Ovando, P. A. Orellana, and S. E. Ulloa, Phys. Rev. B **94**, 155436 (2016).
[24] I. Weymann, J. Phys.: Condens. Matter **29**, 095301 (2017).
[25] M. T. Deng, S. Vaitiekenas, E. B. Hansen, J. Danon, M. Leijnse, K. Flensberg, J. Nygard, P. Krogstrup, and C. M. Marcus, Science **354**, 1557 (2016).
[26] J. Kondo, Prog. Theor. Phys. **32**, 37 (1964).
[27] A. C. Hewson, *The Kondo Problem to Heavy Fermions* (Cambridge University Press, Cambridge, 1993).
[28] D. Goldhaber-Gordon, H. Shtrikman, D. Mahalu, D. Abusch-Magder, U. Meirav, and M. A. Kastner, Nature (London) **391**, 156 (1998).
[29] S. M. Cronenwett, T. H. Oosterkamp, and L. P. Kouwenhoven, Science **281**, 540 (1998).
[30] J. Martinek, Y. Utsumi, H. Imamura, J. Barnaś, S. Maekawa, J. König, and G. Schön, Phys. Rev. Lett. **91**, 127203 (2003); J. Martinek, M. Sindel, L. Borda, J. Barnaś, J. König, G. Schön, and J. von Delft, *ibid.* **91**, 247202 (2003).
[31] R. Lopez and D. Sanchez, Phys. Rev. Lett. **90**, 116602 (2003).
[32] A. N. Pasupathy, R. C. Bialczak, J. Martinek, J. E. Grose, L. A. K. Donev, P. L. McEuen, and D. C. Ralph, Science **306**, 86 (2004).
[33] R. Świrkowicz, M. Wilczyński, M. Wawrzyniak, and J. Barnaś, Phys. Rev. B **73**, 193312 (2006).
[34] M. Sindel, L. Borda, J. Martinek, R. Bulla, J. König, G. Schön, S. Maekawa, and J. von Delft, Phys. Rev. B **76**, 045321 (2007).
[35] J. Hauptmann, J. Paaske, and P. Lindelof, Nat. Phys. **4**, 373 (2008).
[36] I. Weymann and J. Barnaś, Phys. Rev. B **81**, 035331 (2010); I. Weymann and L. Borda, *ibid.* **81**, 115445 (2010).
[37] M. Gaass, A. K. Hüttel, K. Kang, I. Weymann, J. von Delft, and C. Strunk, Phys. Rev. Lett. **107**, 176808 (2011).
[38] I. Weymann, Phys. Rev. B **83**, 113306 (2011).
[39] M. Misiorny, I. Weymann, and J. Barnaś, Phys. Rev. Lett. **106**, 126602 (2011); Phys. Rev. B **84**, 035445 (2011); **86**, 245415 (2012).
[40] K. G. Wilson, Rev. Mod. Phys. **47**, 773 (1975).
[41] K. P. Wójcik, Eur. Phys. J. B **88**, 110 (2015).
[42] R. Bulla, T. A. Costi, and T. Pruschke, Rev. Mod. Phys. **80**, 395 (2008).
[43] We used the open access Budapest NRG code, http://www.phy.bme.hu/∼dmnrg/; O. Legeza, C. P. Moca, A. I. Tóth, I. Weymann, and G. Zaránd, arXiv:0809.3143.
[44] F. B. Anders and A. Schiller, Phys. Rev. Lett. **95**, 196801 (2005); Phys. Rev. B **74**, 245113 (2006).
[45] A. Weichselbaum and J. von Delft, Phys. Rev. Lett. **99**, 076402 (2007).
[46] Y. Meir and N. S. Wingreen, Phys. Rev. Lett. **68**, 2512 (1992).
[47] F. D. M. Haldane, Phys. Rev. Lett. **40**, 416 (1978).